Fire Safety Journal 62 (2013) 289–298

Contents lists available at ScienceDirect

Fire Safety Journal

journal homepage: www.elsevier.com/locate/firesaf

Wildland fire modeling with an Eulerian level set method and automated calibration

Chris Lautenberger *

Reax Engineering Inc., 1921 University Ave. Berkeley, CA 94704, United States

ARTICLE INFO

Article history:
Received 30 January 2013
Received in revised form
28 May 2013
Accepted 4 August 2013
Available online 18 October 2013

Keywords:
Wildland fire modeling
Level set method
Moonlight

ABSTRACT

This paper presents the mathematical development of a geospatial model for simulating wildland fire spread. The Eulerian level set method (LSM), a mathematical technique that tracks interfaces between separate regions on a regular grid, is applied here to track the interface between burned (or burning) areas and green areas. Model physics include surface fire spread rate and direction, transition from surface fire to passive or active crown fire, ember lofting, trajectory tracking, and spot fire formation, acceleration from point ignitions, and modifications to fuel strata attributed to suppression activities. A novel aspect of this work involves application of a stochastic optimization algorithm to automatically calibrate baseline model inputs by comparing calculated fire perimeters to observed (target) fire perimeters. The wildland fire model and associated automated calibration technique are assessed by simulating the first 22 h of progression of the 2007 Moonlight Fire in Northern California. Fuels and topography inputs are obtained from the Landfire project while wind and weather inputs are obtained from high resolution numerical weather prediction. Fire areas simulated with the calibrated model agree well with target perimeters.

1. Introduction

Wildland fire propagation has conventionally been simulated using Lagrangian particles that function as markers or tracers for the fire front. This approach is applied in FARSITE [1] via Huygens principle with the assumption that each point along the fireline propagates independently as an elliptical wavelet. With a Lagrangian approach to tracking wildfire propagation (whether using Huygens principle, the Level Set Method, or another front tracking procedure) the fire perimeter is visualized by connecting adjacent Lagrangian markers. In this category, Fendell and Wolff [2] and Rehm and Mell [3] applied a Lagrangian level set method to simulate wildland fire propagation. Potential disadvantages of Lagrangian front tracking methods include increase of computational requirements as fire size (and therefore the number of markers) grows and, more significantly, the inability of such methods to natively handle fire crossovers and mergers without resorting to complex logic to "fix" such crossovers and mergers.

Eulerian level set methods, commonly used for tracking the demarcation between burned and unburned parcels of gases in premixed combustion simulations, offer several advantages over their Lagrangian counterparts for simulating wildland fire spread. Spot fire formation, fire mergers, and crossovers can all be handled without any special treatment as is required with Lagrangian methods. The underlying numerical method leverages decades of research into numerical solution of hyperbolic partial differential equations, providing a robust and stable solution. Rehm and McDermott [4], Mallet et al. [5], Mandel et al. [6], Kim [7], Lo [8], and Rochoux et al. [9], among others, have applied Eulerian level set methods to simulate wildland fire propagation. Indeed, Eulerian level set methods have been implemented in coupled atmospheric fire models including WRF-FIRE/SFIRE [10] and Wildland Urban Interface Fire Dynamics Simulator (WFDS) [11]. Mandel et al. [6] and Lo [8] have demonstrated application of the Eulerian LSM to simulation of wildland fire spread in complex fuels and terrain.

This paper presents mathematical development of ELMFire (Eulerian Level set Model of Fire spread), an open source geospatial model intended for simulating wildland fire development using an Eulerian level set method [12]. It is intended for simulating wind-driven fires but is not appropriate, in its current form, for simulating plume-dominated fires where air entrainment into the fire plume has a significant impact on the wind speed and direction in the vicinity of the fire front. In order to handle plume-dominated fires, it would be necessary to incorporate a submodel that accounts for interactions between the fire's buoyant convective column and the wind field near the fire front. Model physics include surface fire spread rate and direction, transition from

* Tel.: +1 510 629 4930.
E-mail address: lautenberger@reaxengineering.com

0379-7112/$ - see front matter © 2013 Elsevier Ltd. All rights reserved.
http://dx.doi.org/10.1016/j.firesaf.2013.08.014

surface fire to passive crown fire (where the canopy of a tree or group of trees torches but the flaming is maintained only for a short period of time) or active crown fire (where combustion of the canopy and surface fuels are intimately coupled, leading to continuous and sustained propagation), ember lofting and spot fire formation, acceleration from point fire ignitions, and modifications to fuel strata attributed to suppression efforts (direct attack). Required inputs include geospatial fuels and topography information and a gridded wind/weather stream. Message Passing Interface (MPI) is used to simultaneously execute multiple simulations across distributed memory parallel (DMP) compute resources. This facilitates a novel aspect of this work, and one of the focuses of this paper: automated model calibration using a stochastic optimization routine (and related applications such as Monte Carlo Simulation for sensitivity analysis).

After presenting ELMFire's mathematical development, several verification simulations are presented and fire perimeter shapes are discussed. Finally, the first 22 h of the 2007 Moonlight Fire are simulated after model inputs are calibrated using an optimization technique based on a genetic algorithm, and good agreement between simulated and target perimeters is obtained. It is concluded that automated calibration (perhaps combined with real-time data assimilation and stochastic simulation) appears to have great potential for enhancing predictive capabilities of wildland fire models.

2. Eulerian level set wildland fire model

This section presents the mathematical formulation of ELMFire.

2.1. Eulerian level set method

Implementation of the level set method in this work largely follows Rehm and McDermott [4]. The level set method involves solving the following hyperbolic differential equation for the scalar variable ϕ

$$\frac{\partial\phi}{\partial t}+U_x\frac{\partial\phi}{\partial x}+U_y\frac{\partial\phi}{\partial y}=0 \tag{1}$$

Note that ϕ has no physical meaning other than at the fire front where $\phi=0$. In Eq. (1), U_x and U_y represent the fire spread rate (m/s) in the x and y (East/West and North/South) directions. Calculation of U_x and U_y is discussed in Sections 2.2 and 2.3.

The fire front propagates only normal to itself. Thus, the normal vector of the ϕ field must be calculated as

$$\hat{n}=\frac{1}{|\nabla\phi|}\left(\frac{\partial\phi}{\partial x}\hat{i}+\frac{\partial\phi}{\partial y}\hat{j}\right)=n_x\hat{i}+n_y\hat{j} \tag{2}$$

where the magnitude of the gradient of the ϕ field is

$$|\nabla\phi|=\sqrt{\left(\frac{\partial\phi}{\partial x}\right)^2+\left(\frac{\partial\phi}{\partial y}\right)^2} \tag{3}$$

The solution method proceeds as follows. First, spatial gradients of the ϕ field are approximated with node-centered central differences

$$\left(\frac{\partial\phi}{\partial x}\right)_{i,j}\approx\frac{\phi_{i+1,j}-\phi_{i-1,j}}{2\Delta x} \tag{4a}$$

$$\left(\frac{\partial\phi}{\partial y}\right)_{i,j}\approx\frac{\phi_{i,j+1}-\phi_{i,j-1}}{2\Delta y} \tag{4b}$$

Next, the ϕ field normal vector is calculated with Eqs. (2) and (3). Geometrical relations are used to calculate the angle θ (measured clockwise from North, see Fig. 1) to which the normal vector in Eq. (2) points as follows:

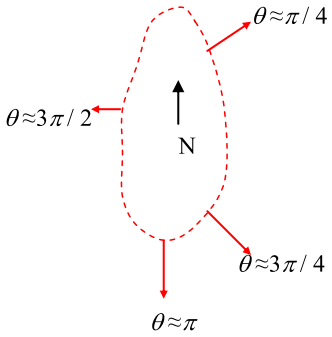

Fig. 1. Graphical illustration of θ, the angle normal to fire front measured clockwise from North, at several locations along a sample fire perimeter.

$$\theta=\begin{cases}\frac{1}{2}\pi-\tan^{-1}\left(\frac{n_y}{n_x}\right) & \text{for } n_x>0 \text{ and } n_y\geq 0\\ \frac{3}{2}\pi+\tan^{-1}\left(\frac{n_y}{|n_x|}\right) & \text{for } n_x<0 \text{ and } n_y\geq 0\\ \frac{3}{2}\pi-\tan^{-1}\left(\frac{n_y}{n_x}\right) & \text{for } n_x<0 \text{ and } n_y\leq 0\\ \frac{1}{2}\pi+\tan^{-1}\left(\frac{|n_y|}{n_x}\right) & \text{for } n_x<0 \text{ and } n_y\leq 0\end{cases} \tag{5}$$

The preceding analysis makes it possible to calculate the fire spread rate at any angle θ, and therefore the components U_x and U_y in Eq. (1), using the methodology that will be described in Sections 2.2 and 2.3.

As suggested by Rehm and McDermott [4], numerical solution of Eq. (1) is accomplished after applying a flux limiter to the convective terms. This ensures solution monotonicity and prevents spurious oscillations that can be induced by the convective terms in the absence of a flux limiter. This, however, necessitates re-calculation of the flux limited spatial gradients of the ϕ field (which are calculated with Eq. (4) solely for the purposes of determining the normal vector in Eq. (2)).

First define the parameter r and the Superbee flux limiter $B(r)$ as [5]:

$$r=\frac{\delta\phi_{up}}{\delta\phi_{loc}} \tag{6}$$

$$B(r)=\max(0,\min(2r,1),\min(r,2)) \tag{7}$$

Partial derivatives with respect to x are defined in terms of "east" and "west" ϕ values, and partial derivatives with respect to y are defined in terms of "north" and "south" ϕ values as

$$\frac{\partial\phi}{\partial x}\approx\frac{\phi_{east}-\phi_{west}}{\Delta x} \tag{8a}$$

$$\frac{\partial\phi}{\partial y}\approx\frac{\phi_{north}-\phi_{south}}{\Delta y} \tag{8b}$$

For the east face:

$$\delta\phi_{loc}=\phi_{i+1,j}-\phi_{i,j} \tag{9.east.1}$$

$$\delta\phi_{up}=\begin{cases}\phi_{i,j}-\phi_{i-1,j} & \text{for } u_{x,i,j}>0\\ \phi_{i+2,j}-\phi_{i+1,j} & \text{for } u_{x,i,j}<0\end{cases} \tag{9.east.2}$$

$$\phi_{east}=\begin{cases}\phi_{i,j}+\frac{1}{2}B(r)\delta\phi_{loc} & \text{for } u_{x,i,j}>0\\ \phi_{i+1,j}-\frac{1}{2}B(r)\delta\phi_{loc} & \text{for } u_{x,i,j}<0\end{cases} \tag{9.east.3}$$

For the west face:

$$\delta\phi_{loc}=\phi_{i-1,j}-\phi_{i,j} \tag{9.west.1}$$

$$\delta\phi_{up}=\begin{cases}\phi_{i-2,j}-\phi_{i-1,j} & \text{for} u_{x,i,j}>0\\ \phi_{i,j}-\phi_{i+1,j} & \text{for} u_{x,i,j}<0\end{cases} \tag{9.west.2}$$

$$\phi_{west} = \begin{cases} \phi_{i-1,j} - \frac{1}{2}B(r)\delta\phi_{loc} & \text{for} u_{x,i,j} > 0 \\ \phi_{i,j} + \frac{1}{2}B(r)\delta\phi_{loc} & \text{for} u_{x,i,j} < 0 \end{cases} \quad \text{(9.west.3)}$$

For the north face:

$$\delta\phi_{loc} = \phi_{i,j+1} - \phi_{i,j} \quad \text{(9.north.1)}$$

$$\delta\phi_{up} = \begin{cases} \phi_{i,j} - \phi_{i,j-1} & \text{for } u_{y,i,j} > 0 \\ \phi_{i,j+2} - \phi_{i,j+1} & \text{for } u_{y,i,j} < 0 \end{cases} \quad \text{(9.north.2)}$$

$$\phi_{north} = \begin{cases} \phi_{i,j} + \frac{1}{2}B(r)\delta\phi_{loc} & \text{for } u_{y,i,j} > 0 \\ \phi_{i,j+1} - \frac{1}{2}B(r)\delta\phi_{loc} & \text{for } u_{y,i,j} < 0 \end{cases} \quad \text{(9.north.3)}$$

For the south face:

$$\delta\phi_{loc} = \phi_{i,j-1} - \phi_{i,j} \quad \text{(9.south.1)}$$

$$\delta\phi_{up} = \begin{cases} \phi_{i,j-2} - \phi_{i,j-1} & \text{for } u_{y,i,j} > 0 \\ \phi_{i,j} - \phi_{i,j+1} & \text{for } u_{y,i,j} < 0 \end{cases} \quad \text{(9.south.2)}$$

$$\phi_{south} = \begin{cases} \phi_{i,j-1} - \frac{1}{2}B(r)\delta\phi_{loc} & \text{for } u_{y,i,j} > 0 \\ \phi_{i,j} + \frac{1}{2}B(r)\delta\phi_{loc} & \text{for } u_{y,i,j} < 0 \end{cases} \quad \text{(9.south.3)}$$

The initial burning area is initialized to a value of $\phi = -1$, and the non-burning areas are initialized to $\phi = 1$. To simulate an already burning fire, a shape (vector) file representing the fire perimeter at a particular point in time can be burned to a raster and used to initialize the simulation, or the user can directly specify point or line type ignitions. Zero gradient boundary conditions are applied at the edges of the computational domain.

As suggested by Rehm and McDermott [4], the solution is marched forward in time using a second order Runge Kutta method

$$\phi^* = \phi^t - \Delta t\left(U_x\frac{\phi^t_{east} - \phi^t_{west}}{\Delta x} + U_y\frac{\phi^t_{north} - \phi^t_{south}}{\Delta y}\right) \quad \text{(10a)}$$

$$\phi^{t+\Delta t} = \frac{1}{2}\phi^t + \frac{1}{2}\left(\phi^* - \Delta t\left(U^*_x\frac{\phi^*_{east} - \phi^*_{west}}{\Delta x} + U^*_y\frac{\phi^*_{north} - \phi^*_{south}}{\Delta y}\right)\right) \quad \text{(10b)}$$

Timetep (Δt) is constrained by the Courant–Friedrichs–Lewy (CFL) condition. The location of the fire perimeter is determined by interpolation of the ϕ field as the level set corresponding to $\phi = 0$. This (and all other) geoprocessing is accomplished using the Geospatial Data Abstraction Library (GDAL) [13].

2.2. Surface fire spread rate

Recall that U_x and U_y in Eq. (1) represent surface fire spread rate in the x and y (East and North) directions. Surface fire spread rate and direction depend on several factors, some of which include: fuel type and loading, moisture content of dead and live fuels, topographical slope and aspect, mid-flame wind speed and azimuth, and fire front configuration. U_x and U_y should be thought of as generic functions of these (and potentially other) variables. Although U_x and U_y can be calculated using several methodologies, the Eulerian level set method that is the focus of this paper is not dependent on use of any particular method for calculating U_x and U_y. However, in the current paper, surface fire spread rate (Section 2.2) and direction (Section 2.3) are calculated from the widely-used Rothermel/Albini modeling techniques published by the US Forest Service [14,15], although it is emphasized that alternative methods for calculating spread rate and direction can be used with this method.

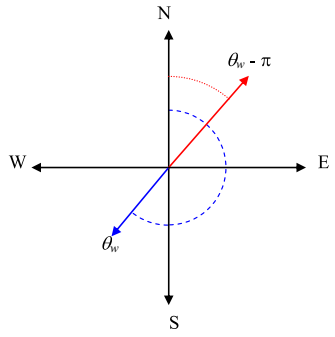

Fig. 2. Wind azimuth θ_w (direction from which wind blows) and $\theta_w - \pi$ (direction to which wind blows).

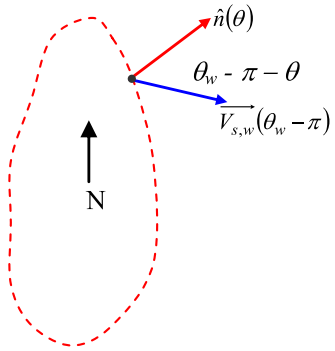

Fig. 3. Fire front normal vector $\hat{n}(\theta)$ and wind-aligned spread rate vector $\overrightarrow{V_{s,w}}$ at a point along fire perimeter. Wind-induced spread rate in direction normal to fire front is found by taking dot product of these two vectors.

Under the Rothermel/Albini paradigm, the magnitude of the surface fire spread rate (V_s, m/s) is calculated as

$$V_{s,Rothermel} = \frac{I_R\xi(1+\phi_w+\phi_s)}{\rho_b\varepsilon Q_{ig}} \quad \text{(11)}$$

where I_R is the reaction intensity (kW/m^2), ξ is the propagating flux ratio (-), ϕ_w and ϕ_s are dimensionless wind and slope factors, ρ_b is bulk density (kg/m^3), ε is the surface heating number (-), and Q_{ig} is the heat of preignition (kJ/kg). The reader is referred to the original publications [14,15] for details.

The surface fire spread rate calculation methodology requires specification of several fuel-specific parameters that are typically established through the use of stylized fuel models that map required parameters to representative fuel complexes. Spatial Geographic Information System (GIS) fuels mappings can be obtained from several sources, including the Landfire project [16].

2.3. Surface fire acceleration

The Rothermel model described above provides the equilibrium rate of surface fire spread, but in reality this equilibrium rate of spread is not achieved instantaneously. Consequently, for initial ignition locations and spot fires that form during a simulation, the rate of spread increases from zero to the equilibrium spread rate as follows:

$$\frac{V_s}{V_{s,Rothermel}} = 1 - \exp\left(-\frac{t - t_{ign}}{\tau_{accel}}\right) \quad \text{(12)}$$

In Eq. (12), t_{ign} is the time (s) at which a pixel is ignited by a user-specified ignition or by spotting, and τ_{accel} is a user-specified acceleration time constant (s), typically on the order of 600 s.

2.4. Surface fire spread rate normal to fire front

Wind direction is normally reported as the direction from which the wind blows, i.e. a wind from angle θ_w, blows toward angle $\theta_w-\pi$. This is shown graphically in Fig. 2. A wind-driven fire is "pushed" toward angle $\theta_w-\pi$. Similarly, aspect (θ_a) is the direction that a slope faces, i.e. an East facing slope has an azimuth of $\theta_a=\pi/2$. A fire burning under the influence of slope is "pulled" upslope toward the angle $\theta_a-\pi$.

Now consider a fire burning in flat terrain and, as shown in Fig. 3, focus on a point on the fire front having a unit normal vector $\hat{n}(\theta)=n_x\hat{i}+n_y\hat{j}=\sin(\theta)\hat{i}+\cos(\theta)\hat{j}$. Consistent with the preceding definitions, assume that wind blows across this segment of the fire front toward the angle $\theta_w-\pi$. The wind induced spread rate in the direction normal to the fire front, i.e. aligned with the angle θ, is found by taking the dot product of the wind-aligned spread rate vector $(\overrightarrow{V_{s,w}}(\theta_w-\pi)=V_{s0}(1+\phi_s)(\sin(\theta_w-\pi)\hat{i}+\cos(\theta_w-\pi)\hat{j}))$ with the fire front's unit normal vector as follows:

$$\begin{aligned}||V_s(\theta)|| &= \overrightarrow{V_{s,w}}(\theta_w-\pi)\cdot\hat{n}(\theta)\\ &= V_{s0}(1+\phi_w)(\sin(\theta_w-\pi)\hat{i}+\cos(\theta_w-\pi)\hat{j})\cdot(\sin(\theta)\hat{i}+\cos(\theta)\hat{j})\\ &= V_{s0}(1+\phi_w)(\sin(\theta_w-\pi)\sin(\theta)+\cos(\theta_w-\pi)\cos(\theta))\\ &= V_{s0}(1+\phi_w)\cos(\theta_w-\pi-\theta)\end{aligned} \tag{13}$$

where the final equality made use of the trigonometric identity $\sin(a)\sin(b)+\cos(a)\cos(b)=\cos(a-b)$.

After conducting the analogous analysis for slope, the magnitude of surface fire spread rate at angle θ (and parallel to the slope) is calculated as

$$\frac{V_s}{V_{s0}}=\max(1,(1+\phi_s\cos(\theta_a-\pi-\theta)+\phi_w\cos(\theta_w-\pi-\theta))) \tag{14}$$

In Eq. (14), V_{s0} is the no wind/no slope spread rate evaluated from Eq. (11) with $\phi_w=0$ and $\phi_s=0$, where ϕ_w and ϕ_s are the Rothermel wind and slope factors in Eq. (11) (not to be confused with the scalar ϕ used in the level set method). The "max" operator in Eq. (14) limits the minimum spread rate normal to the fire front to the no-wind/no slope spread rate.

Since Eq. (14) gives the rate of spread parallel to the slope it must first be projected to map coordinates. Essentially, for fires burning in sloped terrain, the fire area when viewed from directly overhead is less than the true fire area by a factor proportional to $\cos(\gamma)$ where γ is the topographical slope. This means that the spread rate in the uphill (and downhill) direction must be reduced by a factor of $\cos(\gamma)$, but no modification is necessary for spread rate perpendicular to the slope. This is shown graphically in Fig. 4 where V_s is the spread rate parallel to the slope (Eq. (14)) and V_s^* is the spread rate projected to map coordinates.

Since the spread rate in map coordinates is required not just for these two limiting cases (spread up/down slope and perpendicular to the slope) a more general relation is derived from the geometrical relations shown in Fig. 4 as follows:

$$\begin{aligned}\frac{V_s^*}{V_s} &= 1-|\hat{n}(\theta_a-\pi)\cdot\hat{n}(\theta)|(1-\cos(\gamma))\\ &= 1-|\sin(\theta_a-\pi)\sin(\theta)+\cos(\theta_a-\pi)\cos(\theta)|(1-\cos(\gamma))\\ &= 1-|\cos(\theta_a-\pi-\theta)|(1-\cos(\gamma))\\ &= 1-|-\cos(\theta_a-\theta)|(1-\cos(\gamma))\\ &= 1-|\cos(\theta_a-\theta)|(1-\cos(\gamma))\end{aligned} \tag{15}$$

Note the limiting cases for Eq. (15): for $\theta=\theta_a$, $V_s^*/V_s=\cos(\gamma)$ and for $\theta=\theta_a\pm90^\circ$, $V_s^*/V_s=1$ as expected.

The factors U_x and U_y are then calculated from Eqs. (2) and (15) as

$$U_x=n_xV_s^* \tag{16a}$$

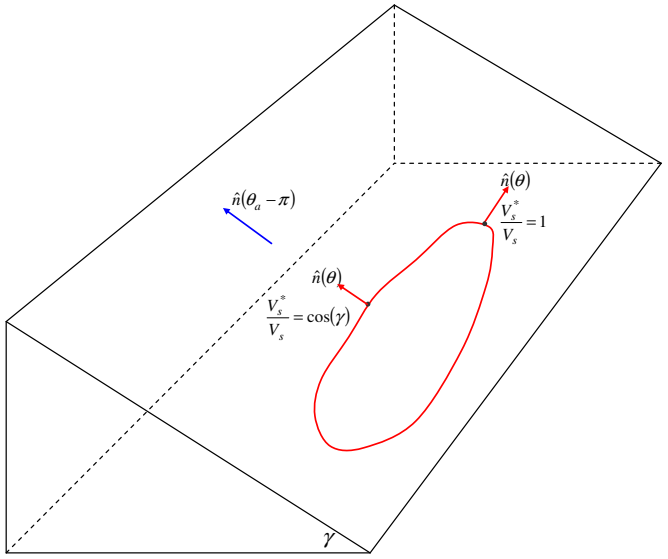

Fig. 4. Fire perimeter in sloped terrain. For fire spreading upslope (and downslope) the spread rate projected to map coordinates (V_s^*) is reduced from the spread rate parallel to the slope ($\boldsymbol{V}_s$) by a factor of $\cos(\gamma)$. Projected spread rate perpendicular to the slope is unaffected.

$$U_y=n_yV_s^* \tag{16b}$$

2.5. Crown fire initiation and spread rate

The critical fireline intensity (I_0, kW/m) for torching is calculated as [17]

$$I_0=(0.01\times\mathrm{CBH}\,(460+26\times M))^{3/2} \tag{17}$$

where 0.01 is "an empirical constant of complex dimensions whose value is to be found from field observations" [17], CBH is canopy base height (m), M is foliar moisture content (%), and 460+26 M is the "heat of ignition" (kJ/kg) [17]. When the fireline intensity of the surface fire exceeds I_0, torching (passive crown fire) occurs. Since the Rothermel/Albini model calculates the fireline intensity of a heading fire, the actual fireline intensity I_{act} (kW/m) for heading, flanking, and backing fires is calculated as

$$I_{act}=I_{head}\frac{V_s}{V_{s,head}}=I_{head}\frac{\max(1,(1+\phi_s\cos(\theta_a-\pi-\theta)+\phi_w\cos(\theta_w-\pi-\theta)))}{1+\phi_s+\phi_w} \tag{18}$$

Following Van Wagner [17], active crown fire occurs only when the spread rate exceeds the critical spread rate required for active crown fire (RAC, m/s)

$$\mathrm{RAC}=\frac{0.05}{\mathrm{CBD}} \tag{19}$$

where CBD is canopy bulk density (kg/m^3), and the constant in the numerator (0.05 kg/m^2 s) was established from experimental crown fire observations [17].

If active crown fire occurs, the spread rate is approximated as 3.34 times the spread rate in Fuel Model 10 with a wind reduction factor of 0.4 [18], although Rothermel's correlation factor (3.34) could be treated as an empirical adjustable parameter to be optimized.

2.6. Dead fuel moisture content

Due to diurnal variations in relative humidity and temperature, dead-fuel moisture content is transient. Dead fuel moisture content is calculated for three timelag/fuel size classes (1-hour, 10-hour, and 100-hour fuels) by numerically integrating the

following first order ordinary differential equation with an explicit Euler method:

$$\frac{dM}{dt}=\frac{M_{eq}-M}{\tau_c} \tag{20}$$

where M_{eq} is the equilibrium moisture content, M is the instantaneous moisture content, t is time, and τ_c is the fuel timelag constant for the corresponding fuel size class (1-hour, 10-hour, or 100-hour). Equilibrium fuel moisture content in Eq. (20) is calculated as in the Fosberg Fire Index (RH in % and T in °F) [19,20]:

$$M_{eq}=\begin{cases}0.03+0.28\times \mathrm{RH}-0.00058\times \mathrm{RH}\times T & \text{for } \mathrm{RH}<10\%\\ 2.23+0.16\times \mathrm{RH}-0.0148\times T & \text{for } 10\le \mathrm{RH}<50\%\\ 21.1-0.4944\times \mathrm{RH}+0.00557\times \mathrm{RH}^2-0.00035\times \mathrm{RH}\times T & \text{for } \mathrm{RH}\ge 50\%\end{cases} \tag{21}$$

Time-dependent relative humidity (RH) and temperature (T) are normally obtained from weather station data, spot forecasts, or Numerical Weather Prediction (NWP) data. The initial moisture content (required to integrate Eq. (21)) can be estimated from local weather station observations. Note that this simple treatment of dead fuel moisture does not account for the possibility of precipitation (rainfall) or condensation (dew) but this could be handled with a more complete treatment of dead fuel moisture such as Nelson's model [21]. This has been addressed by Mandel et al. [22].

2.7. Wind adjustment factor

Wind speeds are normally reported at 20 ft above the vegetative cover in the US and 10 m (32.8 ft) above the vegetative cover internationally. However, wildland fire dynamics calculations (in particular the surface fire spread model described earlier) require as input the wind speed at mid-flame height, which is lower than the 20 ft or 10 m wind speed. The ratio of the mid-flame wind speed to the 20 ft or 10 m wind speed is known as the wind adjustment factor or wind reduction factor. It is generally calculated by assuming that the wind velocity profile ($|u(z)|$) above a vegetative cover (grass, shrubs, or forest) follows a logarithmic profile [23]:

$$|u|=\frac{u_*}{\kappa}\ln\left(\frac{z-D_0}{z_0}\right) \tag{22}$$

where $|u|$ is the wind velocity magnitude (m/s) as a function of height (z, m), u_* is the friction velocity ($u_*=\sqrt{\tau/\rho}$ m/s where τ is the horizontal shear stress (N/m^2) and ρ is the air density (kg/m^3)), κ is von Kármán's constant (0.4, dimensionless), D_0 is the zero-plane displacement (m), and z_0 is the surface roughness length scale (m). In Eq. (22), the zero-plane displacement (D_0) and surface roughness length (z_0) are related to the height (H) of the dominant vegetative cover as follows [23]:

$$D_0=0.64H \tag{23a}$$

$$z_0=0.13H \tag{23b}$$

Substituting:

$$|u|=\frac{u_*}{\kappa}\ln\left(\frac{z-0.64H}{0.13H}\right) \tag{24}$$

The ratio of wind speed at 20 ft to 32.8 ft (10 m) can be calculated from Eq. (24) (with height units in feet instead of meters for convenience) as:

$$\frac{|u_{H+20}|}{|u_{H+32.8}|}=\frac{\frac{u_*}{\kappa}\ln\left(\frac{H+20-0.64H}{0.13H}\right)}{\frac{u_*}{\kappa}\ln\left(\frac{H+32.8-0.64H}{0.13H}\right)}=\frac{\ln\left(\frac{H+20-0.64H}{0.13H}\right)}{\ln\left(\frac{H+32.8-0.64H}{0.13H}\right)} \tag{25}$$

while the ratio in Eq. (25) does vary with height of the vegetative cover, a value of $|u_{H+20}|/|u_{H+32.8}|\approx 0.87$ is accurate to better than ~5% for most vegetation heights. For this reason, this ratio (0.87) is used here to convert 10 m (32.8 ft) wind speed to 20 ft (6.1 m) wind speed.

The methodology used to calculate mid-flame wind speed depends on whether or not a canopy is present. The canopy case is addressed first followed by the no canopy case.

From Eq. (24), the wind speed at the canopy height H is

$$|u_H|=\frac{u_*}{\kappa}\ln\left(\frac{H-0.64H}{0.13H}\right)=\frac{u_*}{\kappa}\ln\left(\frac{1-0.64}{0.13}\right)=\frac{u_*}{\kappa}\ln(2.77)=1.02\frac{u_*}{\kappa}\approx\frac{u_*}{\kappa} \tag{26}$$

The ratio of wind speed at the canopy height H to the wind speed at 20 ft above the canopy is:

$$\frac{|u_H|}{|u_{20+H}|}=\frac{1}{\ln((20+H-0.64H)/0.13H)}=\frac{1}{\ln((20+0.36H)/0.13H)} \tag{27}$$

Below the canopy, the wind speed profile is [23]:

$$|u|=\begin{cases}\frac{u_*}{\kappa}\ln\left(\frac{z-0.64H}{0.13H}\right) & \text{for } z\ge z_m\\ u_c & \text{for } z<z_m\end{cases} \tag{28}$$

where u_c is the characteristic canopy wind speed and z_m is a height near but below the canopy height.

The ratio of below-canopy wind speed to the wind speed at the top of the canopy is [23]:

$$\frac{|u_c|}{|u_H|}=\frac{0.555}{\sqrt{fH}} \tag{29}$$

where f is the crown filling fraction, which is related to canopy cover (CC) for a conical crown shape and rectangular square horizontal tree spacing as

$$f=\mathrm{CC}\frac{\pi}{12} \tag{30}$$

For the case with no canopy present, the ratio of the mid-flame wind speed to the 20-foot wind speed is [23]

$$\frac{|u_{mf}|}{|u_{20+H}|}=\frac{1+0.36H/H_F}{\ln((20+0.36H)/0.13H)}\left(\ln\left(\frac{H_F/H+0.36}{0.13}\right)-1\right) \tag{31}$$

where H_F is the flame extension above the fuel bed. For simplicity, in this work H_F/H is taken as constant and equal to 2, although it could be calculated iteratively from the flame length output by the surface fire spread model.

2.8. Spot fire formation

A simple model for spotting from embers generated by passive or active crown fire is implemented here. This spotting submodel is a hybrid of the classical Albini [24] model and more recent work by Tse, Anthenien, and Fernandez-Pello [25–26]. Individual embers or firebrands are modeled as Lagrangian particles with position governed by the following ordinary differential equation:

$$\frac{d\boldsymbol{x}}{dt}=\boldsymbol{V}_{abs} \tag{32}$$

where $\boldsymbol{x}$ is the particle's position vector (m), $\boldsymbol{V}_{abs}$ is the particle's absolute velocity vector (m/s), and t is time (s). The initial condition is

$$\boldsymbol{x}|_{t=0}=\boldsymbol{x}_0 \tag{33}$$

The time rate of change of a particle's velocity is related to its acceleration as:

$$m\frac{d\boldsymbol{V}_{abs}}{dt}=m\boldsymbol{a}=\boldsymbol{F}_g+\boldsymbol{F}_D \tag{34}$$

where m is the particle's mass (kg), $\boldsymbol{a}$ is its acceleration vector (m/s^2), $\boldsymbol{F}_g$ is the force vector due to gravity (kg m/s^2), and $\boldsymbol{F}_D$ is the force vector due to wind resistance/drag (kg m/s^2). The initial

condition is

$$\boldsymbol{V}_{abs}\big|_{t=0} = \boldsymbol{V}_{abs0} \tag{35}$$

For convenience, particle mass is presented hereafter in terms of particle density and diameter. For a sphere, the assumed particle shape used in this work, the relationship between particle mass (m), volume (V), density (ρ), and diameter (D) is

$$m = \rho V = \rho\frac{\pi}{6}D^3 \tag{36}$$

Similar relationships can be derived for other shapes such as cylinders and disks.

The gravity vector, in SI units, is

$$\boldsymbol{F}_g = mg = -9.8m\hat{\boldsymbol{k}} \tag{37}$$

where g is the acceleration of gravity (9.8 m/s^2 in the $-\hat{\boldsymbol{k}}$ ($-z$) direction). The drag force vector is

$$\boldsymbol{F}_D = -\frac{1}{2}C_D\rho_{air}A_{proj}|\boldsymbol{V}_{rel}|\boldsymbol{V}_{rel} \tag{38}$$

where C_D is the dimensionless drag coefficient, ρ_{air} is the air density, A_{proj} is the particle's projected area, and $\boldsymbol{V}_{rel}$ is the particle's velocity relative to the ambient (freestream) airflow. Relative velocity and projected area (assuming spherical particle shape) are

$$\boldsymbol{V}_{rel} = \boldsymbol{V}_{abs} - \boldsymbol{U}_\infty \tag{39}$$

$$A_{proj} = \frac{\pi}{4}D^2 \tag{40}$$

Here, $\boldsymbol{U}_\infty$ is the local ambient air velocity. The drag coefficient for a sphere is a function of Reynolds number (Re) as follows:

$$C_D = \frac{24}{\mathrm{Re}}(1+0.15\mathrm{Re}^{0.687}) + \frac{0.42}{1+42500\mathrm{Re}^{-1.16}} \tag{41}$$

$$\mathrm{Re} = \mathrm{Re}_D = \frac{\rho_{air}|\boldsymbol{V}_{\boldsymbol{rel}}|D}{\mu_{air}} \tag{42}$$

where μ_{air} is air's (temperature-dependent) viscosity, evaluated at the film temperature, and all other quantities have been defined.

An ember's regression rate is estimated as [25]:

$$\frac{dD^4}{dt} = -3.46K^2t \tag{43}$$

where K is an empirical burning rate constant:

$$K = K^0(1+0.276\mathrm{Re}^{1/2}\mathrm{Pr}^{1/3}) \tag{44}$$

In Eq. (44), K^0 is taken as 1.8×10^{-7} m^2/s [26] and other properties are taken from Refs. 25,26.

The horizontal components of the wind velocity profile is calculated for a given wind speed and azimuth using the methodology described in Section 2.7. The vertical component, $U_{\infty,z}$, is estimated as follows:

$$U_{\infty,z} = \begin{cases} U_{cl}(z) & \text{for } t \le t_{loft} \\ 0 & \text{for } t > t_{loft} \end{cases} \tag{45}$$

where t_{loft} is the loft time, defined here as the time for which an ember is acted upon by the buoyant plume structure generated by torching trees, and $U_{cl}(z)$ is the centerline velocity (m/s) of an axisymmetric Heskestad plume [27] with virtual origin z_0:

$$U_{cl}(z) = 3.4\left(\frac{g}{c_{p\infty}\rho_\infty T_\infty}\right)^{1/3}\dot{Q}_c^{1/3}(z-z_0)^{-1/3} \tag{46a}$$

$$z_0 = z_{fb} - 1.02D_t + 0.083\dot{Q}^{0.4} \tag{46b}$$

z_{fb} is the flame base height, taken as 50% of the canopy height minus the canopy base height, and D_t (torching diameter) is the hydraulic diameter of a group of torching trees. D_t could be estimated from the crown fire type (passive or active) but here it is treated as an empirical parameter and held constant at 5 m for this work. Heat release rate (kW) of a group of torching trees is calculated as:

$$\dot{Q} = \frac{\pi}{4}D_t^2\Delta H_c\frac{(\mathrm{CH}-\mathrm{CBH})\mathrm{CBD}}{t_b} \tag{47a}$$

$$\dot{Q}_c = (1-\chi_r)\dot{Q} \tag{47b}$$

where CH=canopy height (m), CBH=canopy base height (m), CBD=canopy bulk density (kg/m^3), and ΔH_c=heat of combustion ($\sim$18 MJ/kg). Following Albini [24], the burn time (t_b, s) is related to a dimensionless torching time (TT) and flame length (z_f)

$$t_b = \frac{2}{2.3}\mathrm{TT}\sqrt{z_f} \tag{48}$$

Although Albini provides nomographs to estimate these parameters from stand characteristics (such as species type, diameter at breast height, etc.), here TT and z_f are treated as adjustable empirical parameters.

The number of embers generated per torching event, as well as the size distribution of those numbers, are calculated randomly within user-prescribed limits. In this work, spherical brands with diameters between 3 mm and 3 cm are considered. A user-specified ignition probability controls the probability of ignition occurring at the location where an ember larger than 2 mm lands. This approximation could be refined to relate ignition probability to fuel bed characteristics (fuel type, moisture content, fuel bed temperature) and ember size at landing. Spot fires are assumed to ignite with no ignition delay, although the spread rate accelerates from zero to the equilibrium spread rate according to Eq. (12).

2.9. Suppression

Direct attack is simulated by changing the fuel model to a non-burnable fuel model at particular points in space. The user specifies a series of starting and ending coordinates a well as the rate at which the fire line is constructed and all pixels “touched” by the fireline.

3. Model verification

The model's underlying subroutines have been verified and, to the extent possible, numerical calculations have been compared with analogous exact solutions. To limit the length of this paper, only model verification calculations related to implementation of the Eulerian level set method for simulating fire spread (the emphasis of this paper) are presented here. Surface fire spread simulations are conducted for a 2 km by 2 km grid, with 5 m grid spacing (400 grid points in each direction). Baseline input parameters are summarized in Table 1.

Table 1
Parameters used in baseline verification simulations.

Parameter	Value
Fuel model	10
1-hr fuel moisture content	3%
10-hr fuel moisture content	5%
100-hr fuel moisture content	6%
Canopy base height (CBH)	2.0 m
Canopy bulk density (CBD)	0.15 kg/m^3
Canopy height (CH)	40 m
Canopy cover (CC)	70%

3.1. No wind/no slope

Under no-wind, no-slope conditions, surface fire spreads radially in all directions at an equal rate, generating circular fire perimeters. Fig. 5 shows calculated fire perimeters, plotted every 20 min, for 2 h of spread. The fire spreads radially from the point of origin (indicated by a filled circle with a cross) approximately 52 m in all directions, consistent with the no wind/no slope spread rate calculated for these conditions with BehavePlus [28] (26 m/h).

3.2. Flat terrain with wind

Given the canopy characteristics in Table 1, for a 10 m/s wind at a height of 10 m, the mid-flame wind speed is approximately 0.72 m/s. The corresponding spread rate calculated with BehavePlus [28] is 75 m/h. This means that after 2 h of spread, the head fire should have spread 150 m from the origin. In Fig. 6, calculated fire perimeters are shown for three different wind azimuths in flat terrain. In all three cases, the head fire spreads 150 m in 2 h.

3.3. No wind with slope

Fig. 7 shows, in projected map coordinates, calculated fire perimeters for fire spreading up a 30° slope for 2 h with no wind. The rate of spread calculated with BehavePlus [28] is 177 m/h (parallel to the slope). The spread distance parallel to the slope in 2 h is therefore 354 m, but in projected map coordinates it is 350 m × cos(30°)=307 m. This distance matches the distance from the origin to the tip of the head fire in Fig. 7.

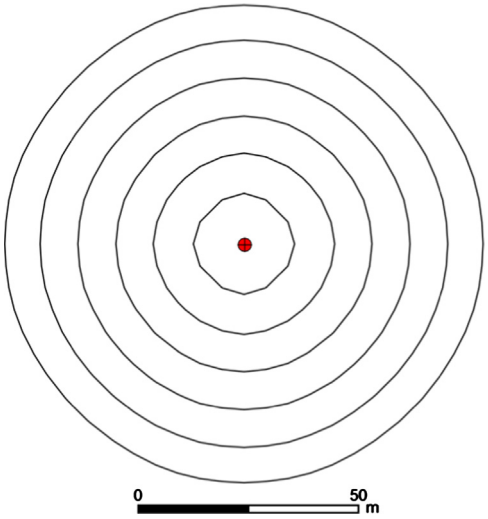

Fig. 5. No-wind/no slope fire perimeter contours.

3.4. Combined wind and slope

Under most conditions, wildland fires spread under the combined influence of slope and wind. Fig. 8 shows calculated fire perimeters for a 2 h of spread on an East facing slope with a 15° angle of inclination and a 10 m/s wind at a height of 10 m coming from an angle of 225°. Although the upslope spread direction is toward 270° and the downwind spread direction is toward 45°, the net effect of slope and wind produces a direction of maximum spread of approximately 4° clockwise from North, consistent with BehavePlus [28] calculations for direction of maximum spread using the Rothermel vectoring approach.

4. Automated calibration algorithm

The concept of model calibration against empirical observations is prevalent in wildland fire modeling. For example, with an emphasis on FARSITE [1], Stratton [29] provides recommendations for calibrating geospatial wildland fire models. In FARSITE [1], calibration is commonly achieved, among other ways, through specification of a spread rate adjustment factor. In this way, over-predictions or under-predictions of spread rate as compared to field observations can be readily rectified. Several additional model inputs can be adjusted from their baseline values in an attempt to improve agreement between model calculations and field observations. If passive crown fire was observed but a simulation shows only surface fire, then parameters that affect onset of torching, such as canopy base height, may require

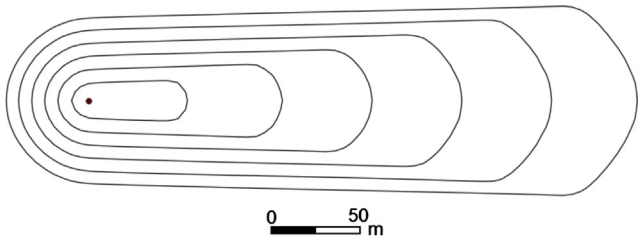

Fig. 7. 20-minute fire perimeters calculated for 2 h of spread in 30° terrain with aspect 270°.

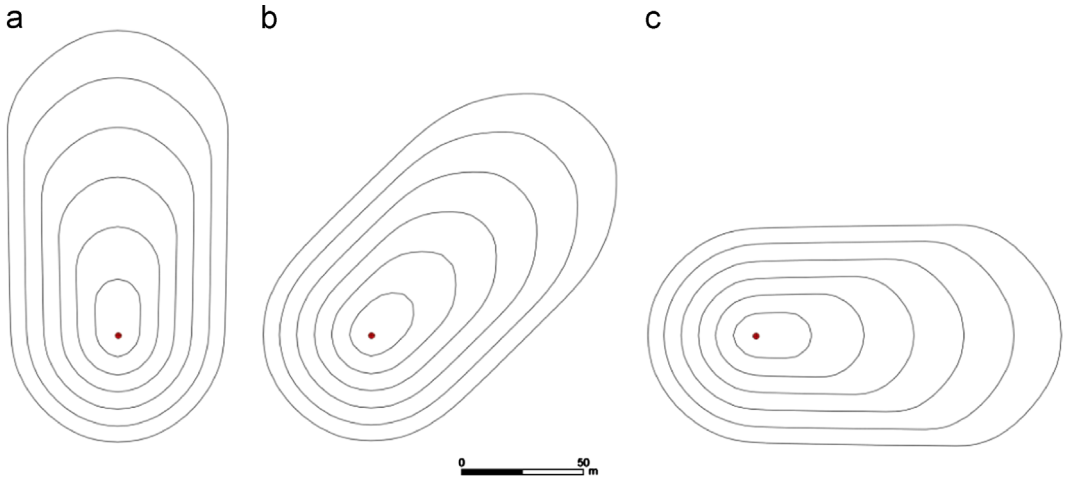

Fig. 6. 20-minute fire perimeters calculated for 2 h of spread in flat terrain with 10 m/s wind at 10 m. (a) 180° wind azimuth. (b) 225° wind azimuth. (c) 270° wind azimuth.

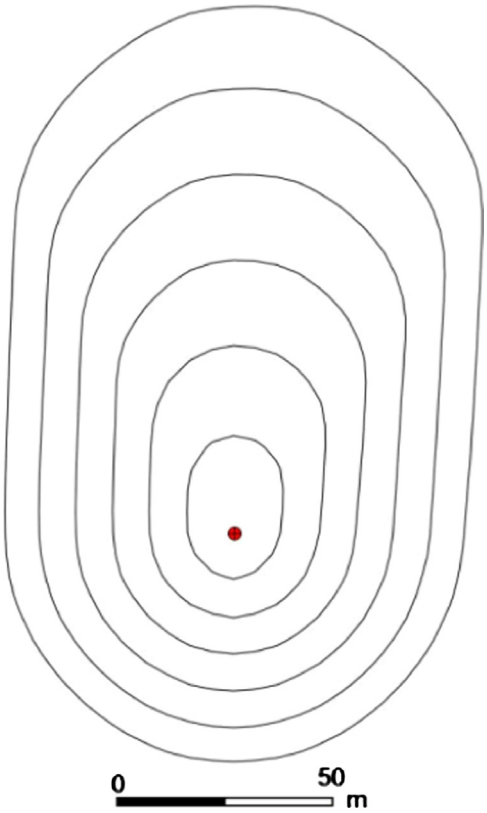

Fig. 8. 20-minute fire perimeters calculated for 2 h of spread. Slope angle is 15° and aspect is 90°. Wind is 10 m/s at height of 10 m from an azimuth of 225°.

adjustment. Similarly, if active crown fire occurred but simulations show only passive crown fire, then an upward adjustment to canopy bulk density may increase the prevalence of active crown fire. Spot fire ignition probability can have a significant impact on overall fire spread, and is typically established by model calibration. Formally, model calibration can be considered a form of inverse modeling where, using the terminology of Jahn et al. [30,31], the simulation is posed as an inverse problem and the invariants (model parameters) are established by optimization. The reader is referred to the work of Jahn et al. [30,31] for additional details.

Wildland fire model calibration is typically accomplished manually. This process involves adjusting an input parameter or parameters, comparing simulated fire progression or spread characteristics to observations, and iterating until model calculations are deemed adequate or no further improvement can be achieved. This manual calibration process is tedious and there is no guarantee that an optimal or near-optimal solution will be found quickly, or at all. However, optimization algorithms are logical tools to automate this model calibration process, thereby reducing turnaround time and ensuring that a near optimal set of calibrated inputs is located. Combined with real time data assimilation from remote sensing techniques or wireless sensors deployed within or near an active fire, optimization algorithms have the potential to significantly improve predictive capabilities of wildland fire models. This has been recognized by Denham et al. [32] who demonstrated the application of a genetic algorithm to optimize wildland fire modeling simulations for a simplified scenario, Rochoux et al. [9] who have demonstrated real time data assimilation during wildland fire spread to improve simulation accuracy, and Rios [33] who combined data assimilation with a tangent linear approach and forward automatic differentiation to solve inverse problems related to wildland fire front propagation.

Table 2
Fitness function applied at each raster point (pixel).

		Simulation	
		Burned	Not burned
Obs.	Burned	1	−1
	Not burned	−1	0

In this work, the ELMFire is linked to a simplified version of the genetic algorithm that has been previously applied by the author and co-workers to estimate material properties for use in pyrolysis modeling [34]. Details of this optimization algorithm are presented elsewhere [34] and are not repeated here.

The fitness function used here compares simulated fire perimeters to actual fire perimeters, pixel by pixel, at known time intervals. The state of each pixel (burned or not burned) in a simulation is compared to the state of the pixel in the fire perimeter used as the calibration target. Scores are then assigned to each pixel as shown in Table 2. If a particular pixel is burned in both the simulation and the target perimeter, that pixel is assigned a score of +1. If a pixel burns in a simulation but not the model, or vice versa, that pixel is assigned a score of −1. If a pixel is not burned in the simulation or the target perimeter, that pixel is assigned a score of 0. The overall fitness at a particular time is then obtained by summing scores over all pixels, and the overall fitness for the entire simulation is obtained by summing over all times for which perimeters are available. Alternate fitness functions could be used, and other fitness metrics such as percent crown consumption could also be included in a composite fitness function.

5. Application to the 2007 Moonlight Fire

The Moonlight Fire was ignited on September 3, 2007 around 2PM in a forested area 10 miles southeast of Westwood, CA. ELMFire and the optimization technique described above are applied here to simulate the first 22 h of the Moonlight Fire using actual topography, fuels, and weather data. Fire spread during this time was wind driven.

Topographical inputs (elevation, slope, and aspect) and fuels inputs (Anderson surface fuel model, canopy cover, canopy bulk density, canopy base height, and canopy height) are obtained from the US Landfire project (LF 1.0.5) [16] at a resolution of 30 m. Wind and weather inputs are obtained from the Weather Research and Forecasting (WRF) mesoscale numerical weather prediction model [35]. The innermost mesh in the WRF simulation has a resolution of 1.2 km. The North American Regional Reanalysis (NARR) [36] dataset is used to initialize WRF and provide lateral boundary conditions. Dead fuel moisture contents are calculated from the WRF weather stream using Eqs. (20) and (21).

Progression of the Moonlight Fire is documented in a US Forest Service publication [37]. Fire perimeters presented in that publication, combined with satellite-based fire detection data (Moderate Resolution Imaging Spectroradiometer, MODIS) [38], are used to develop approximate fire perimeters for use as calibration targets. Near the heel and rear flanks of the fire, fire spread was limited by aerial suppression and direct attack. Therefore, the final Moonlight Fire perimeter obtained from the California Department of Forestry and Fire Protection [39] is specified as a suppression line only in these areas.

Simulations are conducted on a 9 km by 9 km computational domain with 30 m by 30 m grid spacing (300 grid points in each direction). The gridded wind and weather stream is updated at 10 minute intervals from the WRF run. The time of ignition is taken as 2PM and the ignition location is shown as a black dot in Fig. 9. The

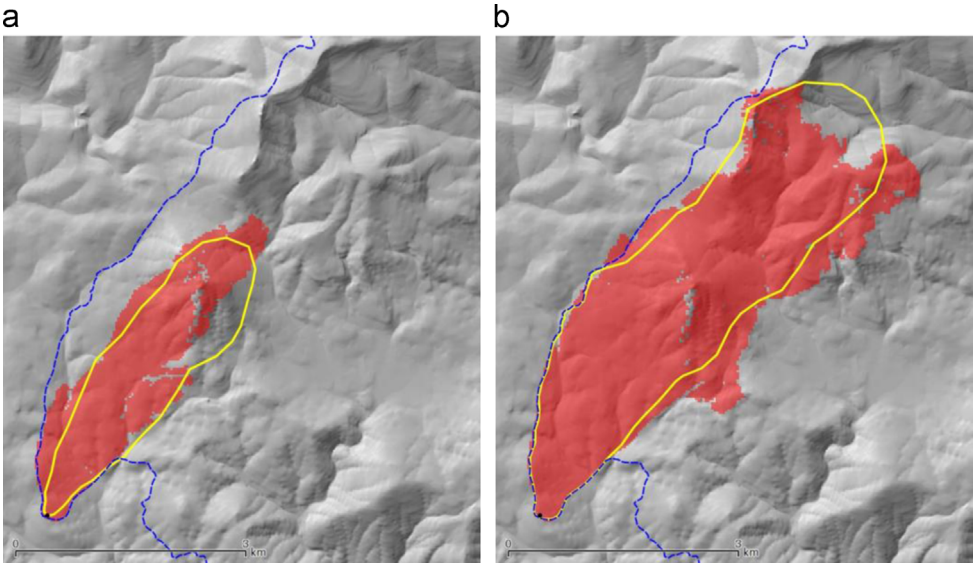

Fig. 9. Comparison of simulated and calibration target perimeters. (a) ~7 h after simulation ignition. (b) ~22 h after simulation ignition. Yellow line indicates target perimeter and red shaded area indicates simulated burned area. Simulation ignition location indicated by black circle. Dashed blue line is Moonlight Fire final perimeter. (For interpretation of the references to color in this figure legend, the reader is referred to the web version of this article.)

Table 3
Input parameters calibrated by genetic algorithm optimization. b=baseline value, i.e. the value at a particular pixel from Landfire [16].

Parameter	Range	Optimal value	Units
Spread rate adjustment factor	[−0.5, 1.5]	1.13	–
Wind reduction factor	[b−0.05, b+0.05]	b+0	–
Canopy bulk density	[b−0.2, b+0.2]	b+0.05	kg/m^3
Canopy base height	[b−3.0, b+3.0]	b−0.50	m
Canopy cover	[b−0.3, b+0.3]	b−0.27	–
TT (torching time)	[3.0, 10.0]	7.7	–
z_F (flame length during torching)	[3.0, 15.0]	9.3	m
t_{loft} (ember lofting time)	[2.0, 20.0]	12	s
P_{ign} (ember ignition probability)	[0.0, 0.2]	0.14	–
# Embers generated per torch	[50, 200]	190	–

ratio of simulated time to wall clock time per CPU core for this particular simulation is approximately 60:1 on an Intel i5 2500 K processor, meaning an hour of simulated fire progression requires approximately 1 min of CPU time. Simulations described in this paper are run in parallel on a 64-core computational cluster, making it possible to simulate the equivalent of approximately 150 days of fire progression per hour of wall clock time.

Table 3 shows the 10 input parameters that are simultaneously calibrated by genetic algorithm optimization, the search range during this optimization process, and the optimal value of each input parameter located by optimization. In Table 3, b denotes "baseline" values (*i.e.*, the value at a particular pixel from Landfire [16]) for spatially varying quantities.

Fig. 9 compares the target and simulated fire perimeter at two times. Fig. 9a compares the simulated and target perimeter at 9:00 PM PDT on September 3, 2007, 7 h after simulation ignition, and Fig. 9b does the same at 12:00 PM on September 4, 2007, 22 h after simulation ignition. By this time, the fire area had grown to approximately 1000 ha. Simulated fire areas agree well with the calibration target perimeters, particularly considering the approximate nature of the target perimeters. Areas along the flanks where the simulation shows burned pixels outside of the target perimeter may be attributed to suppression activities along these flanks that are not included in the simulation. Unburned areas inside the perimeter are rocky areas marked as unburnable in the Landfire data.

6. Concluding remarks

This paper presents the framework for and mathematical development of ELMFire, a geospatial model for simulating wildland fire propagation using an Eulerian level set method. The model has been verified by simulating fire perimeters under idealized conditions and comparing simulated spread distances to expected propagation distances based on BehavePlus [28]. After applying an automated calibration technique based on genetic algorithm optimization, the first 22 h of progression of the 2007 Moonlight Fire is simulated, and good agreement between modeled and calibration target perimeters is achieved.

Although this work demonstrates application of an optimization algorithm to automate calibration of a wildland fire model, the model can also be used for stochastic (Monte Carlo) simulation of wildland fires and sensitivity analyses. Rather than conducting a single simulation, thousands of simulations can be run to assess the effect of uncertainty on various input parameters related primarily to fuels, weather, and spotting, resulting in ensemble predictions. Ultimately, automated calibration, real-time data assimilation, and stochastic simulation could be combined to enhance predictive capabilities; this is one of the long-term motivations for this work.

Future work is planned to systematically assess the impact of various assumptions and modeling approaches on predictive capabilities, computational cost, and required inputs. This will be accomplished by incorporating alternative physics routines that may be invoked at run time. For example, simulations using the Rothermel/Albini surface propagation model or Van Wagner crown fire models could be compared to simulations based on alternative formulations to assess the predictive capabilities of various modeling approaches. It is hoped that disseminating ELMFire as an open source project [12] may stimulate further investigation in these areas.

Acknowledgments

The author would like to thank the anonymous reviewers for providing suggestions that helped strengthen this paper. He would also like to thank Arnaud Trouve, Guillermo Rein, and Oriol Rios for their discussions regarding inverse modeling and data assimilation.

References

[1] Finney, M.A., FARSITE: Fire Area Simulator – Model Development and Evaluation, United States Department of Agriculture Fore Service Rocky Mountain Research Station Research Paper RMRS-RP-4 Revised February 2004.
[2] F.E. Fendell, M.F. Wolff, Wind-Aided Fire Spread, Chapter 6 in Forest Fires, Behavior and Ecological Effects, in: E.A. Johnson, K. Miyanishi (Eds.), Academic Press, San Diego, 2001, pp. 171–223.
[3] R. Rehm, W. Mell, A simple model for wind effects of burning structures and topography on wildland–urban interface surface-fire propagation, International Journal of Wildland Fire 18 (2009) 290–301.
[4] Rehm, R.G. and McDermott, R.J., Fire-Front Propagation Using the Level Set Method, US National Institute of Standards and Technology, NIST Technical Note 1611, March 2009.
[5] V. Mallet, D.E. Keyes, F.E. Fendell, Modeling wildland fire propagation with level set methods, Computers and Mathematics with Applications 57 (2009) 1089–1101.
[6] J. Mandel, J.D. Beezley, A.K. Kochanski, Coupled atmosphere-wildland fire modeling with WRF 3.3 and SFIRE 2011, Geoscientific Model Development 4 (2011) 591–610.
[7] M. Kim, Reaction Diffusion Equations and Numerical Wildland Fire Models (Ph.D. dissertation), University of Colorado Denver Department of Applied Mathematics, 2011.
[8] Shin-en Lo, A Fire Simulation Model for Heterogeneous Environments Using the Level Set Method (Ph.D. dissertation), Claremont Graduate University School of Mathematical Sciences, 2012.
[9] M.C. Rochoux, B. Delmotte, B. Cuenot, S. Ricci, A. Trouve, Regional-scale simulations of wildland fire spread informed by real-time flame front observations, Proceedings of the Combustion Institute 34 (2013) 2641–2647.
[10] ⟨http:/www.openwfm.org/wiki/WRF-Fire⟩.
[11] ⟨http:/www.fs.fed.us/pnw/fera/research/wfds/⟩.
[12] ⟨http:/reaxengineering.com/trac/elmfire/⟩.
[13] ⟨http:/gdal.org/⟩(Geospatial Data Abstraction Library).
[14] Rothermel, R.C., A mathematical model for predicting fire spread in wildland fuels, USDA Forest Service, Research Paper Int-115, January 1972.
[15] Albini, F.A., Estimating wildfire behavior and effects, USDA Forest Service General Technical Report Int-30, 1976.
[16] ⟨http:/landfire.cr.usgs.gov/viewer/⟩.
[17] C.E. Van Wagner, Conditions for the start and spread of crown fire, Canadian Journal of Forest Research 7 (1977) 23–34.
[18] Rothermel, R.C., Predicting behavior and size of crown fires in the Northern Rocky mountains, United States Department of Agriculture Forest Service, Intermountain Research Station, Research Paper Int-438, January 1991.
[19] Simard, A.J., The moisture content of forest fuels – 1. A review of the basic concepts, Canadian Department of Forest and Rural Development, Forest Fire Research Institute, Information Report FF-X-14, Ottawa, Ontario, 47 pp.
[20] S.L. Goodrick, Modification of the Fosberg fire weather index to include drought,, International Journal of Wildland Fire 11 (2002) 205–211.
[21] M.R. Nelson, Prediction of diurnal change in 10-h fuel stick moisture content,, Canadian Journal of Forest Research 30 (2000) 1071–1087.
[22] J. Mandel, J.D. Beezley, A.K. Kochanski, V.Y. Kondratenko, M. Kim, Assimilation of perimeter data and coupling with fuel moisture in a wildland fire – atmosphere DDDAS,, Procedia Computer Science 9 (2012) 1100–1109.
[23] Albini, F.A. and Baughman, R.G., Estimating windspeeds for predicting wildland fire behavior, USDA Forest Service Research Paper Int-221, Intermountain Forest and Range Experiment Station, USDA Forest Service, June 1979.
[24] Albini, F.A., Spot fire distance from burning trees – a predictive model, USDA Forest Service, Intermountain Forest and Range Experiment Station, General Technical Report INT-56, 1979.
[25] S.D. Tse, A.C. Fernandez-Pello, On the flight paths of metal particles and embers generated by power lines in high winds – a potential source of wildland fires, Fire Safety Journal 30 (1998) 333–356.
[26] R.A. Anthenien, S.D. Tse, A.C. Fernandez-Pello, On the trajectories of embers initially elevated or lofted by small scale ground fire plumes in high winds,, Fire Safety Journal 41 (2006) 349–363.
[27] G. Heskestad, Fire plumes, flame height, and air entrainment, Section 2–1, SFPE Handbook of Fire Protection Engineering, fourth ed., National Fire Protection Association, Quincy, MA, 2008.
[28] Andrews, P.L., Bevins, C.D., and Seli, R.C., BehavePlus fire modeling system version 4.0 user's guide, USDA Forest Service General Technical Report RMRS-GTR-106, July 2008.
[29] Stratton, R.D., Guidebook on LANDFIRE fuels data acquisition, critique, modification, maintenance, and model calibration, USDA Forest Service General Technical Report RMRS GTR-220, 2009.
[30] W. Jahn, G. Rein, J.L. Torero, Forecasting fire growth using an inverse zone modelling approach, Fire Safety Journal 46 (2011) 81–88.
[31] W. Jahn, G. Rein, J.L. Torero, Forecasting fire dynamics using inverse computational fluid dynamics and tangent linearisation,, Advances in Engineering Software 47 (2012) 114–126.
[32] M. Denham, K. Wendt, G. Bianchini, A. Cortes, Margalef, Dynamic data-driven genetic algorithm for forest fire spread prediction,, Journal of Computational Science 3 (2012) 398–404.
[33] Rios, O., Forecasting Wind-Driven Wildfires Using An Inverse Modelling Approach, Masters thesis, International Masters in Fire Safety Engineering, University of Edinburgh (Host University), 2013.
[34] C. Lautenberger, G. Rein, A.C. Fernandez-Pello, Application of a genetic algorithm to estimate material properties for fire modeling from bench-scale fire test data, Fire Safety Journal 41 (2006) 204–214.
[35] ⟨http:/www.wrf-model.org/index.php⟩.
[36] ⟨http:/www.emc.ncep.noaa.gov/mmb/rreanl/⟩.
[37] S. Dailey, J. Fites, A. Reiner, S. Mori, Fire behavior and effects in fuel treatments and protected habitat on the moonlight fire, USDA Forest Service (2008) 63.
[38] ⟨http:/activefiremaps.fs.fed.us/data/fireptdata/mcd14ml_2007_conus.htm⟩.
[39] ⟨http://frap.cdf.ca.gov/webdata/data/statewide/fire.dn.zip⟩.